

1
2
3
4
5
6
7
8
9
10

Supplementary information for

**Excitation Wavelength Dependent Quantum Yield in Water Soluble CdTe
Quantum Dots**

*Kush Kaushik,^{a,ξ} Jiban Mondal,^{a,ξ} Ritesh Kumar Bag,^a Shagun Sharma,^a Farhan Anjum,^b
Chayan Kanti Nandi^{a,b,*}*

^aSchool of Chemical Sciences, Indian Institute of Technology Mandi, H.P. -175075, India

*^bSchool of Biosciences and Bioengineering, Indian Institute of Technology Mandi, H.P.
175075, India*

^ξKush Kaushik and Jiban Mondal contributed equally to this work

11 **1.1. Materials**

12 Cadmium chloride hemipentahydrate, $\text{CdCl}_2 \cdot 2.5\text{H}_2\text{O}$, Heavy water (D_2O) and
13 Mercaptosuccinic acid (MSA), were purchased from Sigma. Sodium tellurite was
14 purchased from Alfa-Aesar. Sodium borohydride was purchased from Merck. Hydrazine
15 hydrate 80% was purchased from Loba Chemie private limited. Sulphuric acid and 30%
16 hydrogen peroxide were purchased from fisher scientific. Double-distilled (18.3 M Ω)
17 deionized water was used throughout the entire process.

18 **1.2. Synthesis of CdTe quantum dot solution**

19 CdTe Quantum dots (CQDs) with emission maxima at 604 nm were synthesized following
20 the slightly modified protocol of J. Tan et al., 0.3425 g (1.5 mmol) $\text{CdCl}_2 \cdot 2.5\text{H}_2\text{O}$ was
21 dissolved in deionized water with 0.2477 g (1.65 mmol) MSA, which was then deaerated
22 for 25–30 minutes. The pH of this solution was adjusted to 9–10 using 5 M NaOH. The
23 obtained solution was called solution A. 0.0554 g (0.25 mmol) Sodium tellurite was
24 dissolved separately in 10 mL deionized water and called as solution B. Then, solutions A
25 and B were mixed with 0.0662 g (1.75 mmol) Sodium borohydride. This solution was kept
26 on stirring, and a yellow color solution was obtained after 3–4 minutes, which turned deep
27 orange after fifteen minutes. This solution was then divided into five fractions of 10 mL
28 each, and 400 μL of Hydrazine hydrate 80% was added to each of these fractions for CQDs
29 with ~600 nm emission maxima. These test tubes were then kept on water bath at 90–95
30 $^\circ\text{C}$ for 30 minutes and obtained quantum dots were then allowed to cool under room
31 temperature.

32 **1.3. D_2O - H_2O solvent exchange**

33 Two vials of ~1 mL as synthesised CQDs were freeze-dried/lyophilized for ~14 hours. 0.5
34 mL D_2O and H_2O were used to disperse the lyophilised CQDs. These CQDs were then
35 used for further studies.

36 **1.4. Cell line maintenance, slide preparation and CQDs internalization:**

37 HEK-293t cells were maintained in DMEM media (Gibco) containing 10% fetal bovine
38 serum (Gibco), 1% Penstrap (Gibco), 1% anti-anti and 1% NEA (Gibco) at 37 $^\circ\text{C}$ in
39 humidified CO_2 (5%) incubator. For CQDs internalization inside the cells, healthy HEK
40 cells were seeded on coverslips (prior coated with poly-L-lysine: Sigma) in 2×10^5
41 confluency. After proper adherence cells were washed with 1X PBS buffer and incubated
42 with CQDs for 12 hrs at 37 $^\circ\text{C}$ in humidified CO_2 (5%) incubator. Further cells were

43 properly washed after CQDs incubation and fixed with 4% p-formaldehyde, followed by
44 mounting on a glass slide prior to confocal imaging.

45 **1.5. Steady-state ensemble experiments**

46 **1.5.1. UV-Vis absorption spectroscopy**

47 The UV-Vis absorption spectra were recorded using Shimadzu UV-Vis 2450
48 spectrophotometer. The spectra were collected using a quartz cuvette having a 10 mm path
49 length and 1 ml volume.

50 **1.5.2. Fluorescence spectroscopy**

51 Steady-state fluorescence spectra were recorded on a Horiba fluorolog spectrophotometer
52 and using Agilent Technologies Cary eclipse fluorescence spectrophotometer. Spectra was
53 collected using quartz cuvette of path length 10 mm and 1 mL volume.

54

55 **1.5.3. Fluorescence lifetime (Time-resolved fluorescence decay) spectroscopy**

56 Fluorescence lifetime measurements were performed using Horiba Scientific Delta Flex
57 TCSPC system with interchangeable pulsed LED sources. For this experiment, pulsed LEDs
58 of wavelength 390 nm, 454 nm, 574 nm were used as they lie in the excitation region of
59 CQDs. Ludox has been used to calculate IRF for de-convolution of obtained lifetime
60 spectrum. Horiba DAS6, data analysis software, was used for the fitting of data. Data was
61 fitted using tri-exponential decay function.

$$62 \quad I(t) = \sum_i^n A_i e^{-\left(\frac{t}{\tau_i}\right)}$$

63 Where $I(t)$ is the counts at time t , τ_i is the lifetime value of i^{th} component. A_i is the amplitude of i^{th}
64 component, and n are the number of components

$$65 \quad \tau_{avg} = \frac{\sum_i^n A_i \tau_i^2}{\sum_i^n A_i \tau_i}$$

66 Where τ_{avg} is the average lifetime value obtained using relation.

67

68 **1.5.4. Absolute QY determination using integrated sphere method**

69 We performed the absolute quantum yield measurements using integrating sphere approach
 70 on a QuantaMaster 8450-22 Spectrofluorometer (Horiba) instruments situated at
 71 Sophisticated Analytical and Technical Help Institutes (SATHI), IIT Delhi. CQDs were
 72 ensured to have absorbance < 0.1 at all excitation wavelengths to reduce any artifacts. For
 73 a particular wavelength e.g. for 390 nm excitation, an emission spectrum was taken from
 74 380 nm to 700 nm (scattering and emission part combined) firstly for solvent (water) and
 75 then with CQDs. Same settings were employed for both measurements. Then the excitation
 76 part (excitation $\lambda \pm 10$ nm) and emission part (500-700 nm) of the graphs were integrated
 77 separately for solvent (ref) and sample (CQDs).

78 Absolute quantum yield is represented as the following equation

$$79 \quad \text{Absolute quantum yield} = \frac{\text{Total number of photons emitted}}{\text{Total number of photons absorbed}}$$

80 Therefore, the equation can be reformulated to

$$81 \quad \text{Absolute quantum yield} \\ 82 \quad = \frac{\int(\text{Emission curve for sample}) - \int(\text{Emission curve for solvent})}{\int(\text{Excitation curve for solvent}) - \int(\text{Excitation curve for sample})}$$

83 Using this equation, “Felix GX 4.9.0.10329” software calculated the reported absolute
 84 quantum yield values.

85
86

87 **1.5.5. Radiative and non-radiative decay measurements**

88 From the fluorescence lifetime and QY values, radiative and non-radiative rates were
 89 calculated using the following relations.

$$90 \quad QY = \frac{k_r}{k_r + k_{nr}}$$

$$91 \quad \text{Since, } \tau = \frac{1}{k_r + k_{nr}}$$

$$92 \quad QY = \tau \times k_r$$

$$93 \quad \text{on rearranging } k_r = \frac{QY}{\tau}$$

94 also k_{nr} can be calculated as,

95

$$k_{nr} = \frac{1}{\tau} - k_r$$

96

where, k_r = radiative rate, k_{nr} = non-radiative rate, τ = fluorescence lifetime

97

1.6. Single particle level experiments

98

1.6.1. Fluorescence correlation spectroscopy (FCS)

99

100

101

102

103

104

105

106

107

108

Nikon Eclipse Ti inverted microscope with 60x water immersion objective was used to excite a drop of very diluted (nM) solution of CQDs. The drop was placed over a glass coverslip with thickness ~ 0.1 mm. The emission from sample was directed to a combination of hybrid photomultiplier detector assembly (Picoquant, GmbH Berlin, Germany) placed at 90 degrees from each other. A 600/50 nm bandpass filter was used to filter the emission from CQDs. The filtered light is then directed to both detectors through a 50:50 beam splitter. Then the signal received on one detector is cross correlated to other detector. The signal was analysed and fitted in the Symphotime 64 software supplied with the instrument. Triplet fitting model was used to fit the data obtained from all the excitations.

$$G(t) = \left[1 + T \left[e^{-\left(\frac{t}{\tau_{trip}}\right)} - 1 \right] \right] \sum_{i=0}^{n-1} \frac{\rho(i)}{\left[1 + \frac{t}{\tau_{Diff}[i]} \right] \left[1 + \frac{t}{\tau_{Diff}[i] \kappa^2} \right]}$$

109

110

111

112

113

114

115

Where, τ_{trip} is the triplet state lifetime, τ_{Diff} is the diffusion time of fluorophore from the confocal volume, T is the triplet fraction, n is the number of fluorescing species, $\rho(i)$ is the contribution of i^{th} species. This instrument is equipped with 405, 488, and 561 nm continuous wave lasers, which were used to excite the samples. The laser power of all lasers was calculated over the objective before starting the experiment to take equal power of all lasers with the help of ThorLabs PM160 optical power meter.

116

117

118

119

120

Then, FCS measurements were conducted using a pulsed laser source with a wavelength of 532 nm and a repetition rate of 2 MHz. To obtain information at the single-particle level, the average number of colloidal quantum dots (CQDs) within the confocal volume was maintained below 1, specifically around 0.85 to 0.95. The intensity-time traces of the quantum dots (QDs) as they diffused through the confocal

121 volume were analyzed further for lifetime characterization at different intensity levels,
122 utilizing the SymphoTime 64 software.

123 **1.6.2. Total correlation in FCS and fluorescence antibunching measurements**

124 Total correlation FCS (from lifetime of fluorophore i.e. nanoseconds to seconds) and
125 antibunching experiments were performed at SATHI Facility, IIT Delhi using
126 Picoquant MicroTime 200. This instrument consists of PDL 828 Sepia II, MultiHarp
127 150, an Olympus inverted microscope with 60x water immersion objective and a laser
128 combining unit with 405, 485, 532 nm pulsed diode laser. Microtime 200 system was
129 used in T2 mode with sync killed. A drop of very diluted CQDs sample (average
130 number of particles < 0.6) was kept over glass coverslip. Then the excitation laser in
131 CW mode was focused at the sample, emitted light was observed with two detector
132 setups (both Excelitas single photon counting module SPCM AQRH single photon
133 avalanche photo diode). For observing correlation below microseconds range, we need
134 to use the two-detector system and can only be done in T2 mode with sync killed.
135 separate 582/64 BP filters were used in front of both detectors. Data acquisition was
136 done for nearly one hour. The observed data was then analysed using total correlation
137 and antibunching analysis scripts in Symphotime 64 software.

138

139 **1.6.3. Cleaning of glass coverslips**

140 Since the single particle experiments are very sensitive to the contamination, utmost
141 care was taken to ensure that the glass coverslips were clean. Glass coverslips were
142 treated with Piranha solution (3:1 solution of Sulphuric acid and Hydrogen peroxide)
143 for half an hour, then the mixture was discarded, and glass coverslips were washed with
144 ultrapure deionized water for 4 times and then were ultrasonicated. This process was
145 repeated 4 times. Then the coverslips were kept in water till they were required for the
146 experiment. Freshly cleaned glass coverslips were used for all the experiments. Two
147 empty glass coverslips were analysed for testing impurities to ensure the cleanliness of
148 glass coverslips.

149 **1.6.4. Single particle fluorescence experiments**

150 **1.6.4.1. Single particle fluorescence spectroscopy data acquisition**

151 CQDs solution was first diluted at nM to pM concentration, and the sample was spin-
152 coated over a glass coverslip at ~5000 RPM (with 500 RPM/s acceleration). The

153 coverslip was then mounted over a home-built inverted Nikon Ti epifluorescence
154 microscope objective 100x, 1.49 NA, TIRF objective. Laser beams of wavelengths 488
155 nm, and 532 nm were aligned for simultaneous measurements. The laser beam reaches
156 the glass coverslip using a 590 nm high pass dichroic mirror (AHF analysentechnik) for
157 both 488 nm and 532 nm lasers. After the sample is excited by these lasers, the emission
158 is collected using the same objective. Then, the excitation beam and emission is
159 separated by the same dichroic mirror, i.e., 590 nm high pass filter. Emission is then
160 further filtered using a band pass filter of 580 ± 35 nm. Emission is finally collected at
161 Andor EMCCD iXon Ultra 897. Andor Solis 64-bit software was used to record the
162 data. EMCCD was used in photon counting mode with an EM gain 300, exposure time
163 50 ms (~20 fps), and pixel readout rate 17 MHz. A movie with above mentioned
164 settings, with 5000 frames (~250 s) was recorded and saved in. FITS format. In the
165 recorded video, one pixel corresponds to 160 nm x 160 nm area and an area of 20.48
166 $\mu\text{m} \times 20.48 \mu\text{m}$ (128 x 128 pixels) was recorded.

167 **1.6.4.2. Single particle fluorescence spectroscopy data analysis**

168 The area of the recorded video is $20.48 \mu\text{m} \times 20.48 \mu\text{m}$, and this huge area contains 30-
169 70 number of CQDs particles, and they show intensity fluctuations across the recorded
170 video duration. We custom-built a script using ImageJ macro language to analyse the
171 total photon counts and ON-OFF dwell times for 300-400 individual CQDs. This script
172 first identifies the bright QDs by using maximum intensity projection (Z-project of
173 ImageJ), and NanoJ-core's peak localization (Nearest neighbour analysis). Then a ROI
174 box of 7 x 7 pixels is created around all of these identified localizations, and then the
175 intensity vs. time graph is extracted for individual QDs. These obtained curves are
176 single-particle raw time traces. Now a threshold is set up on all QDs to separate the ON
177 and OFF states. Above the threshold, all emissions are considered ON and below a
178 threshold value, all intensity fluctuations are considered to be OFF. All of these ON and
179 OFF times are noted and photon counts are also extracted from all of such single-
180 particle time traces. A fit line shows the ON states; for OFF states, the fit line reaches
181 zero. It was ensured that no two ROI box overlap each other, in such cases, the ROIs
182 are discarded from the study. An ON time is considered as the time a CQD particle
183 spent in ON state without turning OFF. An OFF time is the time between two
184 subsequent ON-states. If a CQD turns dark and do not turn ON to the end of acquisition,
185 that time is excluded from the OFF state.

186 All photon counts, and ON-OFF dwell times are then recorded in a separate Excel file.
187 Total photon counts are histogrammed and fitted using exponential decay in data
188 analysis and plotting software Origin. ON-OFF dwell times are then histogrammed with
189 50 ms bins and plotted in log-log scales, and fitted using power law and truncated power
190 law equations.

191 Inverse power law: $P_{event} = a \times t_{event}^{-m}$

192 Truncated power law: $P_{event} = a \times t_{event}^{-m} \times e^{-kt_{event}}$

193 Where P_{event} is the probability of event (ON or OFF) time t and k is the inverse of
194 truncation time t_c

195 **1.6.4.3. Power density equalization for 488 nm and 532 nm lasers**

196 To study the effect of excitation wavelength over single particle blinking and photon
197 counting statistics, it was ensured that the power density of lasers (488 nm and 532 nm)
198 were same. This was done to avoid any effect of laser power/intensity on fluorescence
199 blinking, which is already known and reported for several QDs.

200 At first, the laser power was monitored over the objective using a power meter
201 (Thorlabs PM160) for both lasers. Then the output power (obtained from power meter)
202 and input power (given from software) were plotted and fitted. Now we can determine
203 the output power for any input. Since power density is given as

204
$$Power\ density = \frac{Output\ laser\ power}{Area\ of\ laser\ incidence}$$

205 Now to get the area of incidence of the laser on the glass coverslip, we took images of
206 glass coverslip, keeping the output power same for both lasers. Then we measured the
207 area of incidence using ImageJ. We back-calculated the output laser power needed to
208 equate the power density of two lasers using the fitted equation of output power vs input
209 given by software.

210 For this experiment, power density was kept at 0.0107 kW/cm² (or 10.68 W/cm²).

211 **1.6.4.4. Number calculation study**

212 Maximum-intensity projection images were made with the help of ImageJ. Then with
213 the help of a custom-built ImageJ macro language script, all signals were localized, and

214 there locations were marked. Then an ROI (rectangular selection) of 7x7 pixels is made
 215 around all identified signals. The non-overlapping and aggregated CQDs were removed
 216 from the counting of bright CQD particles. Then the number of CQDs were counted.

217 **1.7. Relationship between QY (ensemble) and no of bright particles (single**
 218 **particle)**

$$219 \quad QY^{Bulk} = \frac{\text{Photons emitted by Bright CQDs} + \text{Photon emitted by dark CQDs}}{\text{Photons absorbed by Bright CQDs} + \text{Photon absorbed by dark CQDs}}$$

$$220 \quad \text{Photons emitted by dark CQDs} = 0$$

$$221 \quad QY^{Bulk} = \frac{\text{Photons emitted by Bright CQDs}}{\text{Photons absorbed by Bright CQDs} + \text{Photon absorbed by dark CQDs}}$$

222 *Dividing whole equation by 'Photons absorbed by bright CQDs'*

$$223 \quad QY^{Bulk} = \frac{\text{Photons emitted by Bright CQDs}}{\text{Photons absorbed by Bright CQDs}} \dots \text{eqn 1}$$

$$224 \quad = \frac{\text{Photons emitted by Bright CQDs}}{\text{Photons absorbed by Bright CQDs} + \frac{\text{Photon absorbed by dark CQDs}}{\text{Photons absorbed by Bright CQDs}}}$$

225 Quantum yield of bright fraction can be written as

$$226 \quad QY^{Bright \text{ fraction}} = \frac{\text{Photons emitted by Bright CQDs}}{\text{Photons absorbed by Bright CQDs}}$$

227 *therefore, equation 1 can be rewritten as*

$$228 \quad QY^{Bulk} = \frac{QY^{Bright \text{ fraction}}}{1 + \frac{\text{Photon absorbed by dark CQDs}}{\text{Photons absorbed by Bright CQDs}}}$$

229 Based on the assumption that both dark and bright CQDs absorb in similar fashion

$$230 \quad QY^{Bulk} = \frac{QY^{Bright \text{ fraction}}}{1 + \frac{\text{Dark fraction}}{\text{Bright fraction}}}$$

$$231 \quad QY^{Bulk} = \frac{QY^{Bright \text{ fraction}}}{\frac{\text{Bright fraction}}{\text{Bright fraction}} + \frac{\text{Dark fraction}}{\text{Bright fraction}}} = \frac{QY^{Bright \text{ fraction}}}{\frac{\text{Bright fraction} + \text{Dark fraction}}{\text{Bright fraction}}}$$

$$232 \quad \therefore \text{Bright fraction} + \text{Dark fraction} = 1$$

$$233 \quad QY^{Bulk} = \frac{QY^{Bright\ fraction}}{\frac{1}{Bright\ fraction}}$$

$$234 \quad \therefore QY^{Bulk} = Bright\ fraction \times QY^{Bright\ fraction} \dots eqn\ 2$$

$$235 \quad \gg QY^{Bulk} \propto Bright\ fraction \propto no\ of\ bright\ particles$$

236

237 **1.8. Relationship between apparent rates and intrinsic rates of fluorescent bright** 238 **fractions**

239 *From eqn 2,*

$$240 \quad QY = Bright\ fraction \times QY^{Bright\ fraction}$$

$$241 \quad QY = (1 - D) \times QY^B \dots eqn\ 3$$

242 *Where B = Bright fraction, D = Dark fraction,*

243 *QY = observed quantum yield, QY^B = QY of bright fraction*

$$244 \quad QY = k_r^{App} \times \tau^{App} \text{ and } QY^B = k_r^B \times \tau^B$$

245 *Where, k_r^{App} = Apparant radiative rate, k_{nr}^{App} = apparant non radiative rate,*

246 *k_r^B, k_{nr}^B = Intrinsic radiative, and non radiative rate of bright fraction*

247 *But since the lifetime is independent of the dark fraction for CdTe QDs*

$$248 \quad \tau^{App} = \tau^B = \tau$$

$$249 \quad k_r^{App} = B \times k_r^B \text{ or } = (1 - D) \times k_r^B \dots eqn\ 4$$

$$250 \quad \tau = \frac{1}{k_r^{App} + k_{nr}^{App}} = \frac{1}{k_r^B + k_{nr}^B}$$

$$251 \quad k_{nr}^{App} = \frac{1}{\tau} - k_r^{App} = \frac{1}{\tau} - (1 - D) \times k_r^B$$

$$252 \quad k_{nr}^{App} = \frac{1}{\tau} - (1 - D) \times \left(\frac{1}{\tau} - k_{nr}^B \right)$$

$$253 \quad \text{on rearranging, } k_{nr}^{App} = \frac{D}{\tau} + (1 - D) \times k_{nr}^B \dots eqn\ 5$$

254 Equation 4 and 5 gives the relationship between apparent rates and the intrinsic rates of bright
 255 fraction. We have also added a discussion in ‘Results and discussion’ section of the manuscript.

256 Dependency of dark fraction on apparent rates can be seen from the special cases when there
 257 is no dark fraction (Dark fraction = 0), and when there is no bright fraction (Dark fraction = 1).

258 When dark fraction is absent, equation 4 yields

$$259 \quad k_r^{App} = (1 - D) \times k_r^B = (1 - 0) \times k_r^B$$

$$260 \quad k_r^{App} = k_r^B \dots eqn 6$$

261 Also, when D=0, equation 5 becomes,

$$262 \quad k_{nr}^{App} = \frac{D}{\tau} + (1 - D) \times k_{nr}^B = \frac{0}{\tau} + (1 - 0) \times k_{nr}^B$$

$$263 \quad k_{nr}^{App} = k_{nr}^B \dots eqn 7$$

264 Equation 6, and 7 shows that in the absence of dark fraction, both radiative and non-radiative
 265 apparent rates are the actual rates of bright fraction only.

266 Now, when the whole solution comprises of dark fraction only (no bright fraction), D = 1

267 Equation 4 becomes

$$268 \quad k_r^{App} = (1 - D) \times k_r^B = (1 - 1) \times k_r^B$$

$$269 \quad k_r^{App} = 0 \dots eqn 8$$

270 Equation 5 becomes

$$271 \quad k_{nr}^{App} = \frac{D}{\tau} + (1 - D) \times k_{nr}^B = \frac{1}{\tau} + (1 - 1) \times k_{nr}^B$$

$$272 \quad k_{nr}^{App} = \frac{1}{\tau} \dots eqn 9$$

273 Equation 8 shows that when there is no bright fraction, the apparent rate of complete solution
 274 is independent of the radiative rate of bright fraction and equals to zero. Equation 9 shows that
 275 k_{nr}^{App} is inversely proportional to the fluorescence lifetime of solution only. But this must be

276 considered that for a non-fluorescent solution i.e., $D=1$ and $B=0$, the fluorescence lifetime
277 cannot be defined and hence the k_{nr}^{App} is undefined and independent to k_{nr}^B .

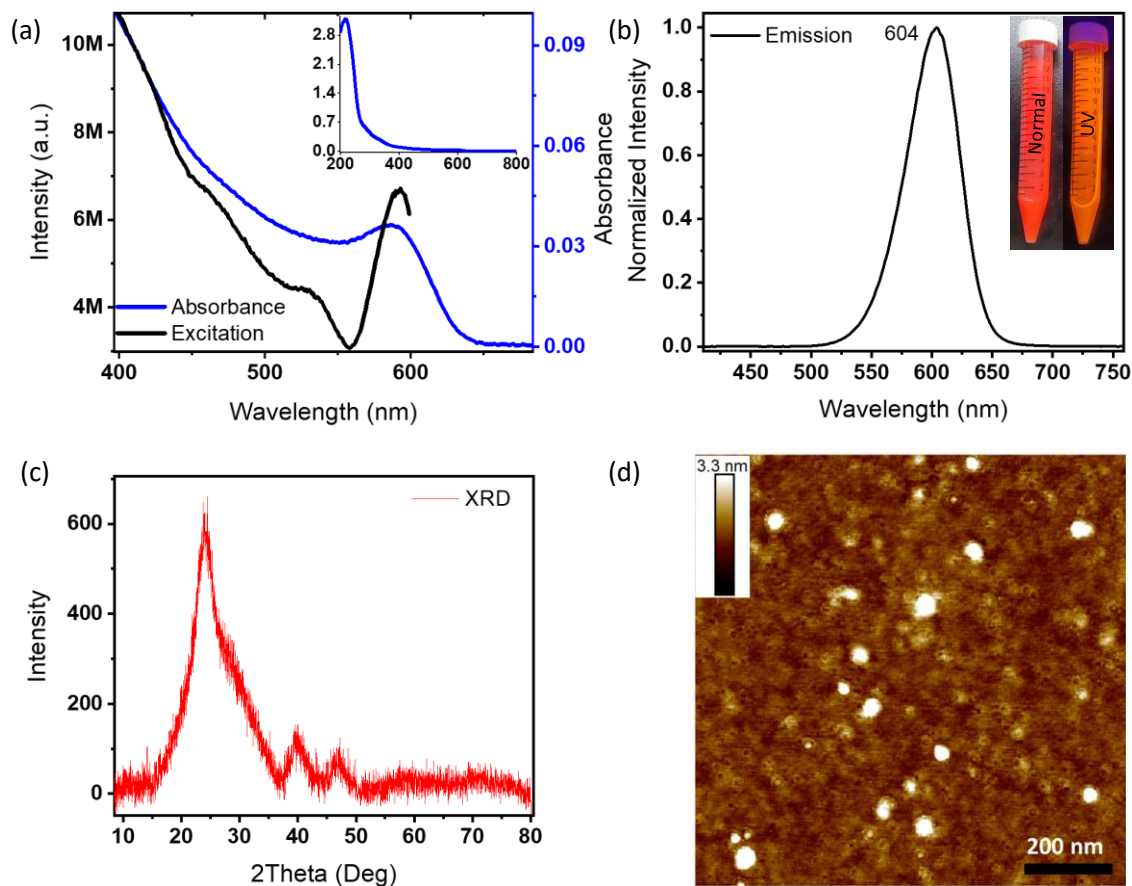
278

279 **1.9. Extrapolation of fluorescence lifetime values at 488 nm, and 532 nm excitations**

280 For performing the fluorescence lifetime experiment, our setup has 390 nm, 454 nm, 574 nm
281 pulsed excitation sources. We extrapolated the value of fluorescence lifetime at 488 nm, and
282 532 nm excitation. Since, there exist very less difference in the fluorescence lifetime spectra at
283 all excitation, the values at 488 nm, and 532 nm should not be much different then the other
284 excitation values. For obtaining the extrapolated values, experimental lifetime values were
285 plotted with excitation wavelengths. Then the plotted points were linear fitted. Then the
286 lifetime values at 488 nm, and 532 nm were obtained from the fitted curve.

287

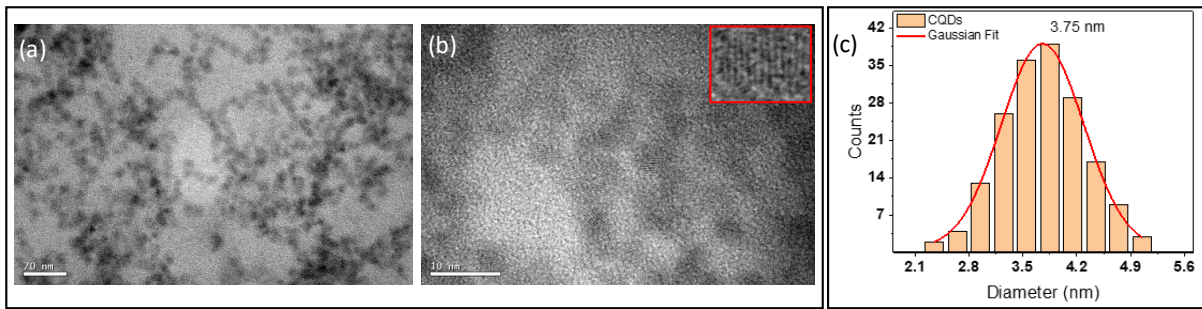
288 **Supplementary figures**



289

290 **Fig. S1:** Photophysical characterization of synthesized water-soluble CQDs: (a) UV-Vis absorption spectrum
 291 (Blue) and fluorescence excitation spectrum (Black) of CQDs with band edge peak at 587 nm, inset shows the
 292 full wavelength absorption spectrum, (b) fluorescence emission spectrum obtained by 390 nm excitation
 293 wavelength with peak maxima at 604 nm. Inset shows photographs of CQDs under normal white light and UV
 294 light excitation. (c) shows the powder XRD analysis of freeze-dried CQDs. (d) AFM height profile data of CQDs
 295 spin-coated over Si wafer.

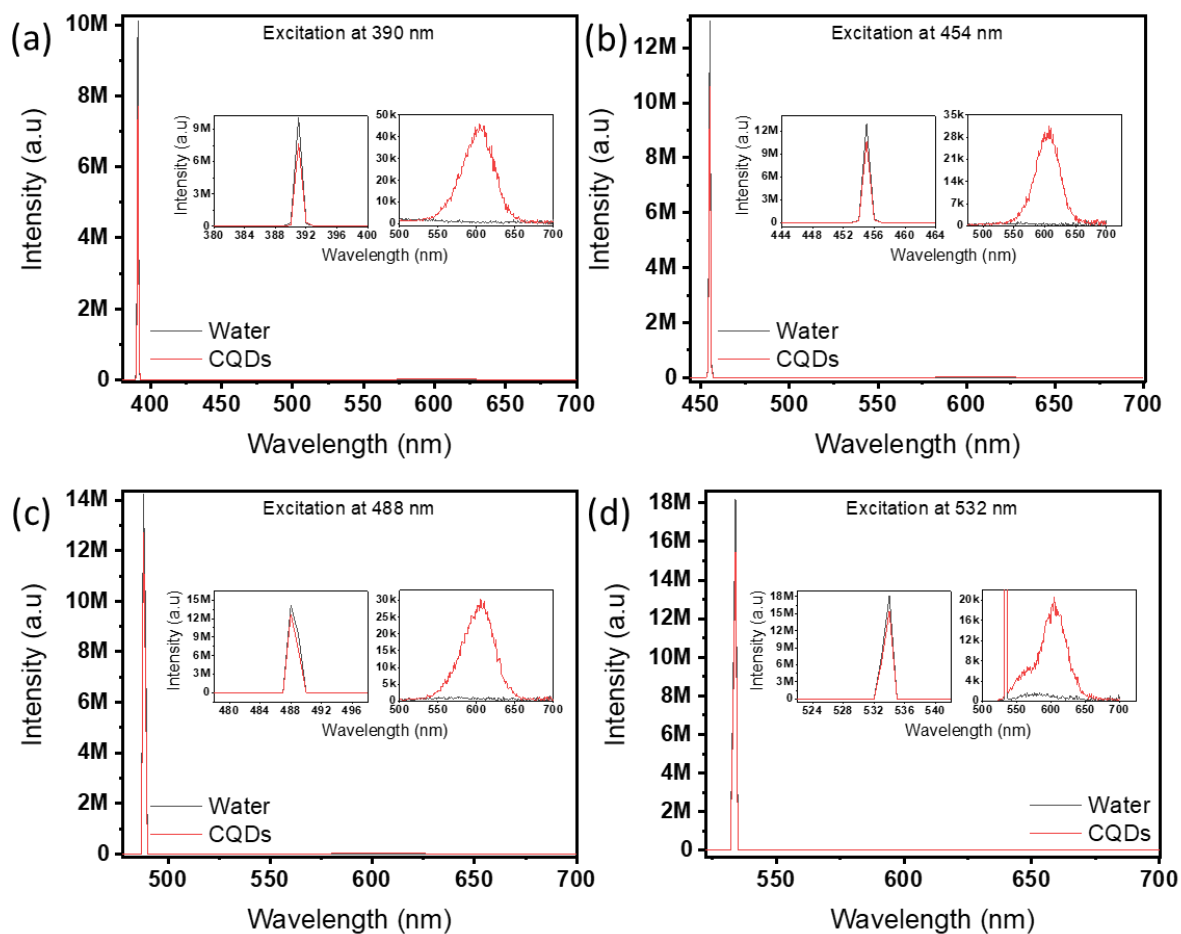
296



297

298 **Fig. S2:** (a, b) TEM micrograph images showing the uniform distribution of sizes of CQDs. (b) inset shows lattice
 299 fringe with size ~ 0.3 nm for CdTe. (c) showing particle size distribution obtained from ~ 175 individual CQDs
 300 with standard deviation of 0.52 nm. Scale bar: 20 nm and 10 nm in (a) and (b) respectively.

301

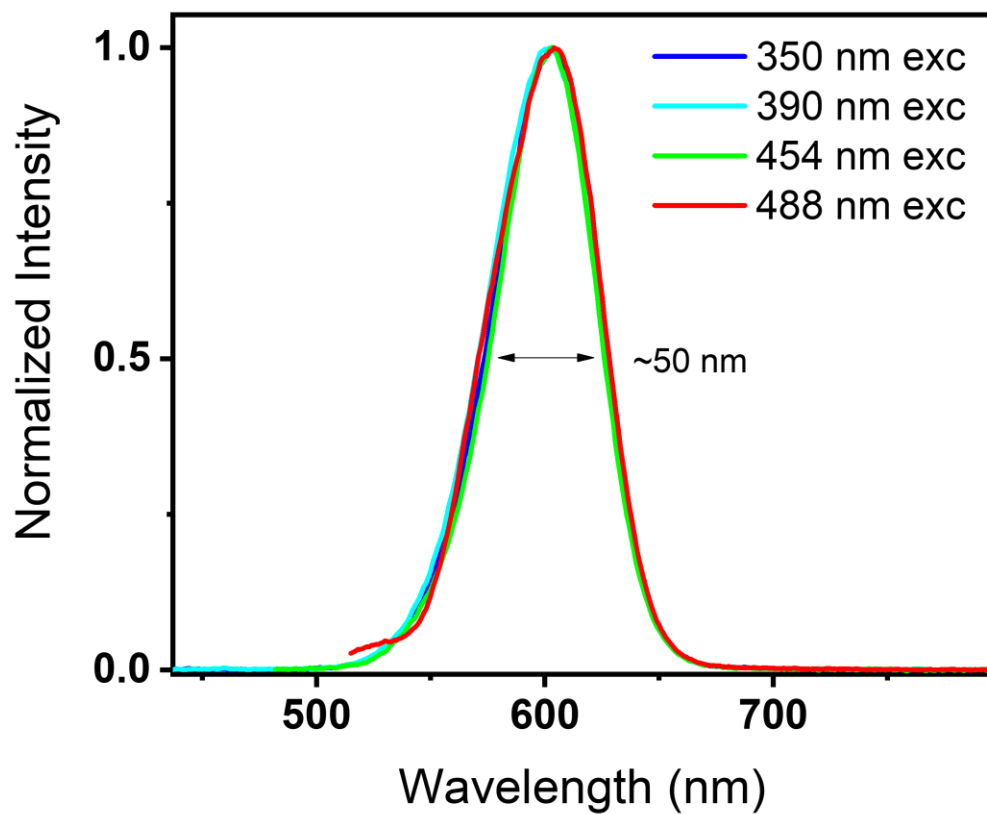


302
 303 **Fig. S3:** Complete range (excitation and emission) spectrum taken keeping the CQDs solution inside integrating
 304 sphere and exciting the sample with (a) 390 nm, (b) 454 nm, (c) 488 nm, and (d) 532 nm. Black curve is for
 305 solvent i.e. water and red curve is for CQDs. inset shows zoomed curves at the excitation range (excitation $\lambda \pm 10$
 306 nm) and emission range (500-700 nm).

307

308 **Table S1:** Absolute quantum yield graph integration values for solvent (ref) and CQDs (sample) at excitation
309 wavelength range (excitation $\lambda \pm 10$ nm) and emission wavelength range (500-700) at various excitations

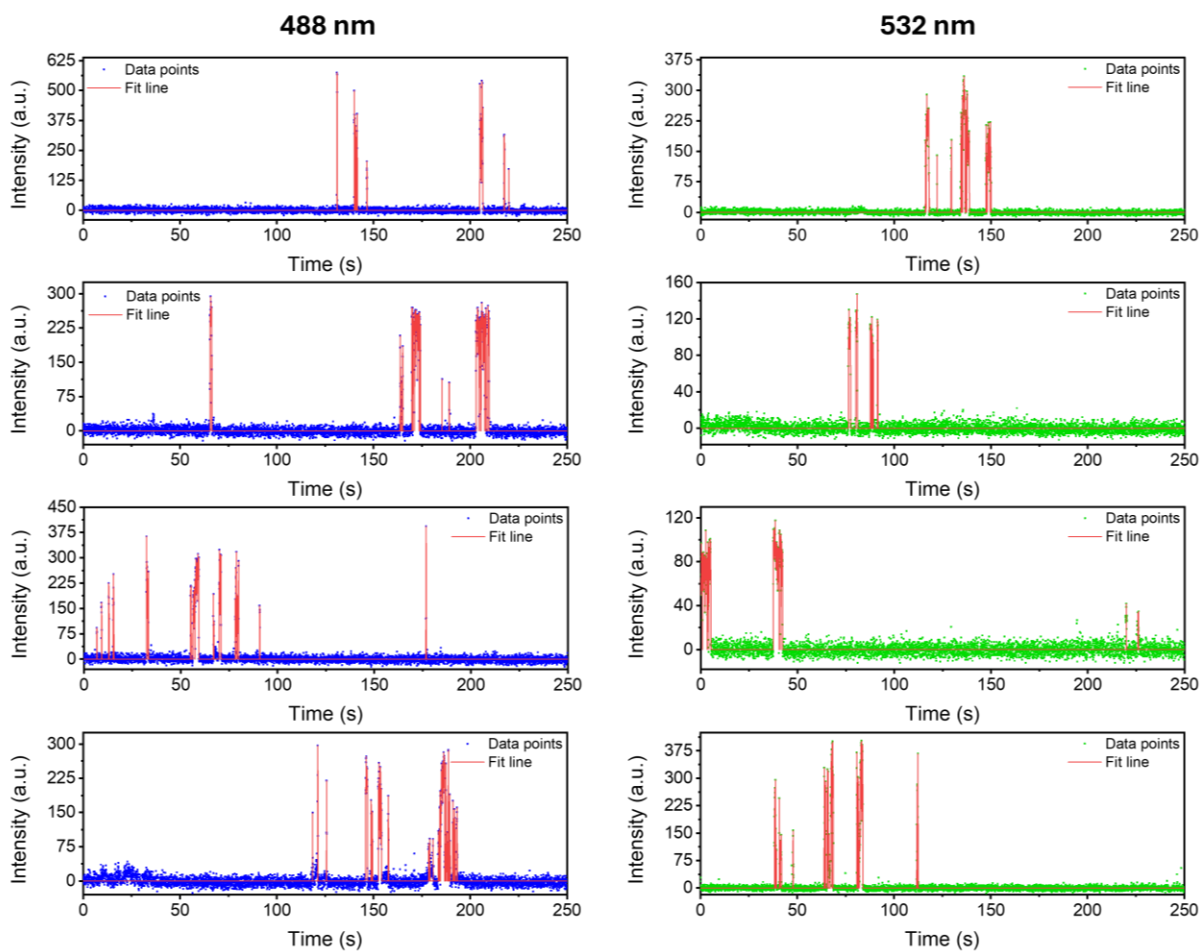
Exc (nm)	$\int I_{em}[\text{CQDs}]$	$\int I_{em}[\text{ref}]$	$\int I_{ex}[\text{CQDs}]$	$\int I_{ex}[\text{ref}]$
390	2363313	143882	9115139	11861320
454	1509863	88115.23	12527510	15324570
488	1532335	105343.1	22067910	26582710
532	958763.6	95440.09	22346560	26214710



310

311 **Fig. S4:** Normalized excitation wavelength dependent emission spectra showing homogeneous emission profile
312 with narrow emission spectrum of full width half maximum of ~50 nm.

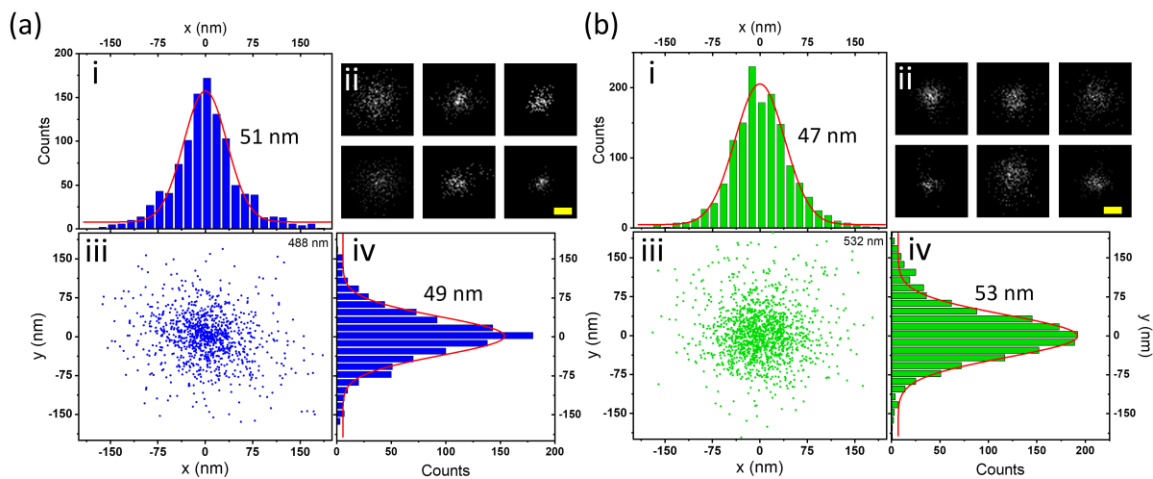
313



314

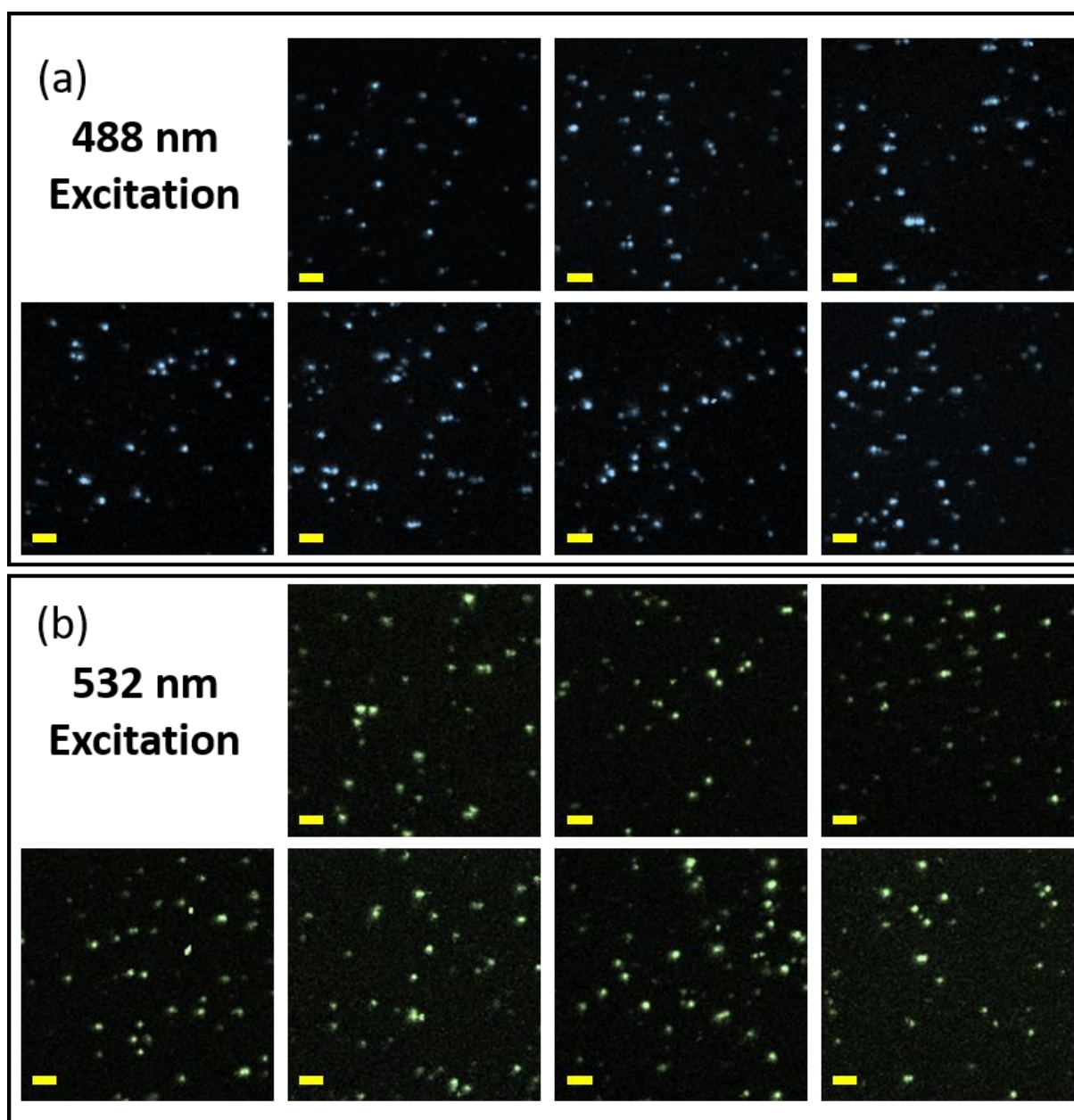
315 **Fig. S5:** Some representative intensity time traces obtained from individual CQDs excited with 488 nm (left panel)
 316 and 532 nm excitation (right panel)

317

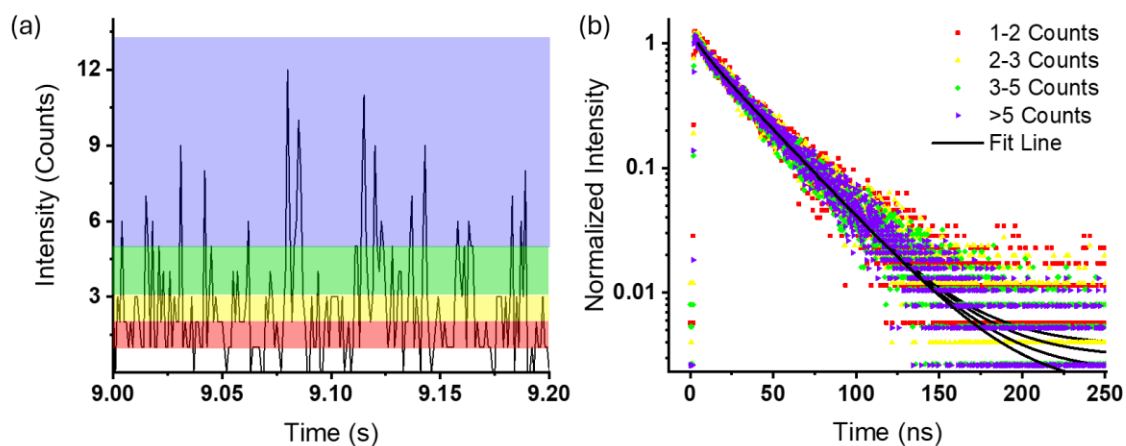


318

319 **Fig. S6:** (a, b) shows the experimental localization precision determination at both 488 nm & 532 nm excitations.
 320 The scatter plot (a, b) (iii) is obtained by the localization of ~ 8 QDs keeping the center of mass of localizations at
 321 origin. (a, b) (i & iv) shows distributions of these localizations along x and y-direction. (iv) shows distributions
 322 of these localizations in y direction. (a, b) (ii) shows representative individual localizations obtained from
 323 Thunder-STORM used for localization precision study. Fit line in (i & iv) shows Gaussian distribution with
 324 standard deviation values ~ 50 nm. Scale bar in single localizations (ii) is 100 nm.

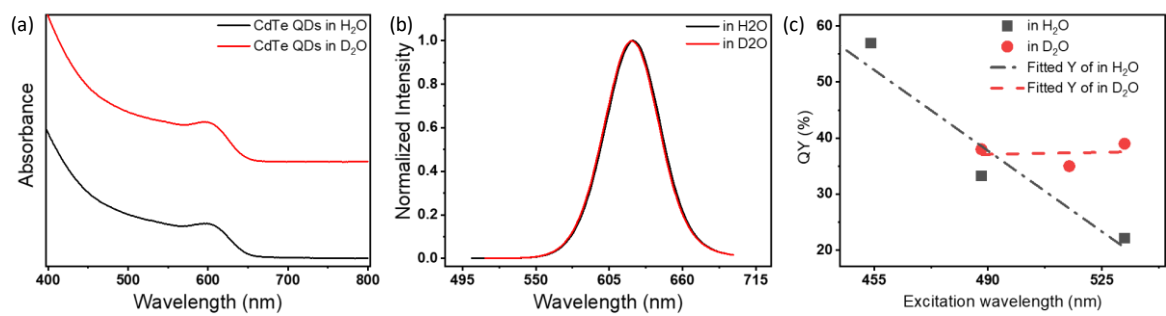


326 **Fig. S7:** Max intensity projection of videos recorded for single particle studies under 488 nm and 532 nm
327 excitations with the same power density. Image area is 20.48 μm x 20.48 μm, Scale bar: 2 μm.



329

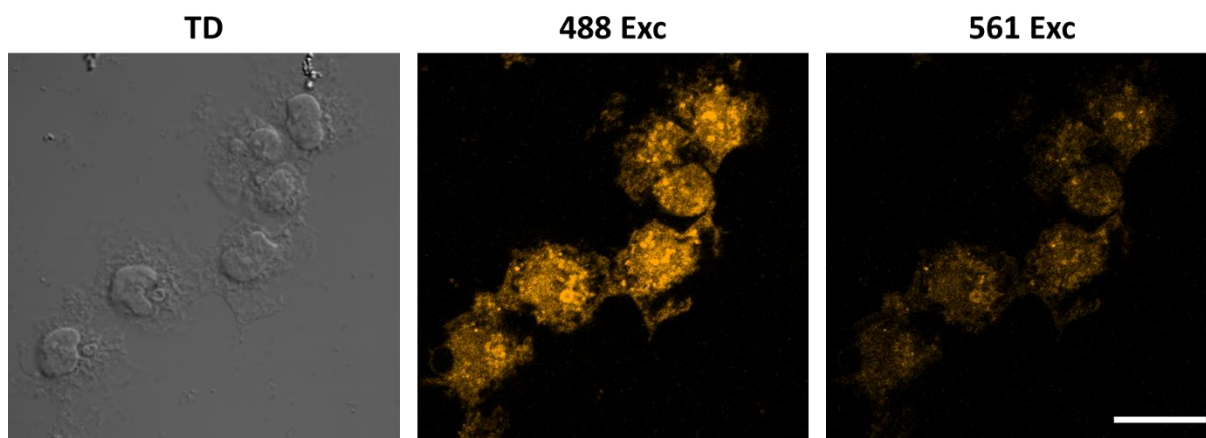
330 **Fig. S8:** (a) Fluorescence intensity–time traces of quantum dots (QDs) diffusing through a confocal volume under
 331 pulsed excitation at 532 nm recorded with an average particle count of closely ~ 1 in the confocal volume to isolate
 332 single-particle intensity fluctuations. The complete measurement time was ~ 60 s. Shaded regions indicate
 333 different intensity states analyzed for fluorescence lifetime measurements. (b) Fluorescence lifetimes
 334 corresponding to the intensity states highlighted in (a). The data reveal that all intensity states exhibit the same
 335 fluorescence lifetime, thus suggesting emission from single emitter species.



336

337 **Fig. S9:** CdTe QDs were redispersed in H₂O (Black) and D₂O (Red) after freeze drying. (a) UV-Vis absorption
 338 spectra (offset for better view), (b) overlapping normalized emission spectrum. (c) Excitation wavelength
 339 dependent QY for QDs in water and excitation independent QY for QDs dispersed in D₂O.

340



341

342 **Fig. S10:** Confocal laser scanning microscope image taken of CdTe QDs stained HEK cells. Samples were excited
343 with 488 nm and 561 nm lasers, and emission was collected in the TRITC channel (595/50 bandpass) with the
344 same detector setting, keeping the excitation laser power at 3.5 μW . High intensity can be observed under 488 nm
345 excitation in comparison to 561 nm excitation. Scale bar: 20 μm .

346